Available online at www.sciencedirect.com
SCIENCE DIRECT
Tetrahedron
ELSEVIER
Tetrahedron 62 (2006) 4071–4080

A quantum chemical study on the mechanism of chiral *N*-oxides-catalyzed Strecker reaction

Zhishan Su, Changwei Hu,* Song Qin and Xiaoming Feng*

Key Laboratory of Green Chemistry and Technology (Sichuan University), Ministry of Education, College of Chemistry, Sichuan University, Chengdu 610064, China

Received 8 September 2005; revised 8 February 2006; accepted 8 February 2006

Available online 6 March 2006

Abstract—The mechanism for the Strecker reaction of silyl cyanide (H_3SiCN) and benzaldehyde *N*-methylimine ($PhCH{=}NCH_3$) catalyzed by chiral 3,3′-dimethyl-2,2′-bipyridine *N*,*N*′-dioxide was investigated using the density functional theory (DFT) at the B3LYP/6-31G* level. The calculations revealed that the non-catalyzed reaction proceeded in a concerted way via a five-membered ring transition state, while the catalytic one occurred stepwisely via a hexacoordinate hypervalent silicate intermediate. It was predicted that both non-catalyzed and catalytic Strecker reactions involved two competitive reaction pathways, that is, addition followed by isomerization or isomerization followed by addition. The calculations indicated that two reaction pathways were comparable for both non-catalyzed and catalytic Strecker reactions. In the catalytic reaction, the strong electron donor (N–O) of chiral *N*-oxide played an important role in enhancing the reactivity and nucleophilicity of H_3SiCN by coordinating O atom to the Si atom of H_3SiCN. Chiral *N*-oxide could be used as a good catalyst for the reaction, which was in agreement with the experimental observations.

1. Introduction

Unnatural α-amino acids are expected to play key roles in improving the original properties and the functions of proteins; therefore, the development of efficient methods for the preparation of various types of α-amino acids has attracted considerable attention.[1] Recently, the hydrocyanation of imine (asymmetric Strecker reaction) has become one of the most intensively studied reactions because it is one of the most direct and viable strategies for the asymmetric synthesis of α-amino acids, which involves the reaction of cyanide with imines to produce α-amino nitriles—key intermediates for the synthesis of α-amino acids.[2–4] Several kinds of catalysts have been developed to obtain various α-amino nitriles using Strecker reaction.[5–12] Amine *N*-oxides are one of the most important catalysts among them.[2,13] Because of possessing notable electron-pair donating property,[14,15] amine *N*-oxides have been used in Strecker reaction as efficient catalysts to produce various α-amino nitriles with high yields under mild and practical conditions.[2,13]

A plenty of investigations suggested that the amine *N*-oxides exhibited significant nucleophilicity toward the silicon by coordinating Si atom to *N*-oxides[2,13] to form hypervalent silicon species with high reactivity. Nakajima and co-worker have employed the chiral biquinoline *N*,*N*′-dioxide in asymmetric reaction of aldehydes with allyltrichlorosilanes. The results suggested that the allylation proceeded via cyclic chair-like transition structure, involving hypervalent siliciate where one of two *N*-oxides occupied an axial position. Our previous experimental researches demonstrated the interaction between *N*-oxides and TMSCN by NMR information, and hypervalent silicon intermediate were predicted to be formed in the system.[13] Compared with the widely experimental studies, theoretical investigations on the Strecker reaction are currently very limited. And detailed catalytic performance of amine *N*-oxides in the Strecker reaction remains theoretically unclear.

To understand the mechanism of the Strecker reaction catalyzed by chiral *N*-oxides and provide useful information for the rational design and synthesis of new chiral *N*-oxides catalysts, theoretical investigations on the detailed mechanism for the reaction of benzaldehyde *N*-benzhydrylimine ($PhCH{=}NCHPh_2$) and trimethylsilyl cyanide (TMSCN) (Scheme 1) were performed using the B3LYP method in the present work.

Keywords: Strecker reaction; Chiral *N*-oxide; α-Amino nitriles; Hypervalent silicate.
* Corresponding authors. Tel./fax: +86 28 85411105 (C.H.); tel./fax: +86 28 8541 8249 (X.F.);
e-mail addresses: chwehu@mail.sc.cninfo.net; xmfeng@scu.edu.cn; gchem@scu.edu.cn

0040–4020/$ - see front matter © 2006 Elsevier Ltd. All rights reserved.
doi:10.1016/j.tet.2006.02.019

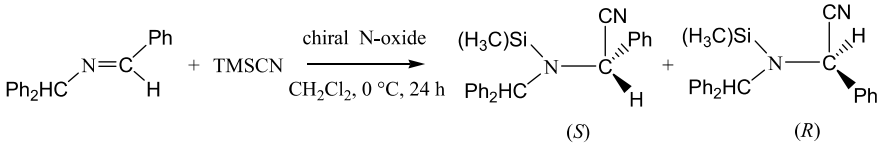

Scheme 1. The Strecker reaction catalyzed by chiral *N*-oxide.

2. Models and computations

Theoretical investigation aiming at the nature of the real catalytic processes based on quantum chemistry approach using gas phase model reaction has been shown to be a useful tool. Because the complexity of the real reaction system causes difficulties for high level computation, investigation on the gas phase reaction of small molecules as model has been adopted and provided very useful information on the reaction mechanism,[16–21] and some successful modeling computations have been performed on the Strecker reaction,[22–25] In the present work, therefore, model molecules were also employed to investigate the mechanism for the Strecker reaction of benzaldehyde *N*-benzhydrylimine ($PhCH{=}NCHPh_2$) and trimethylsilyl cyanide (TMSCN) catalyzed by chiral *N*-oxide **A**. As shown in Scheme 2, silyl cyanide (H_3SiCN) and 3,3′-dimethyl-2,2′-bipyridine *N*,*N*′-dioxide (**B**) were used, respectively, to substitute for TMSCN and 3,3′-dimethyl-2,2′-biquinoline *N*,*N*′-dioxide (**A**), and benzaldehyde *N*-methylimine ($PhCH{=}NCH_3$) (**D**) was used to substitute for benzaldehyde *N*-benzhydrylimine ($PhCH{=}NCHPh_2$) (**C**).

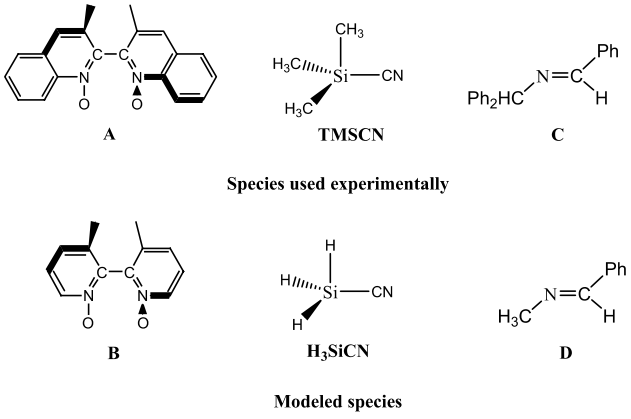

Scheme 2. Real molecules (**A**, TMSCN, **C**) and the corresponding model molecules (**B**, H_3SiCN, **D**) used in the present work.

All calculations were carried out using the Gaussian 03 program.[26] The geometries of all the reactants, products, intermediates and transition states for the Strecker reaction of benzaldehyde *N*-methylimine and H_3SiCN were optimized using the B3LYP method with the 6-31G* basis set. It was rather difficult to carry out intrinsic reaction coordination (IRC) calculation for such a large system. Hence, to confirm the relation between intermediates and transition states, the vibrational modes analysis corresponding to the unique imaginary frequency was adopted. In order to take into account the solvent effect, we also employed the self-consistent reaction field (SCRF) method based on the polarized continuum model (PCM)[27] for the Strecker reaction of benzaldehyde *N*-methylimine and H_3SiCN at B3LYP/6-31G* level. Unless otherwise specified, the single-point energies obtained in CH_2Cl_2 were used in the following discussion. In addition, natural bond orbital (NBO) analysis[28] was performed to obtain a further insight into the mechanism.

3. Results and discussion

The total energies and relative energies of various species in the $PhCH{=}NCH_3 + H_3SiCN$ reaction calculated at the B3LYP/6-31G* level were listed in Table 1. The optimized geometries of various species were depicted in Figures 1–4. In the present work, four reaction pathways (**a** to **d**) were involved. The energy diagrams along the reaction pathways from **a** to **d** were shown in Figures 5 and 6. Selected dominant Wiberg bond indices for each stationary point were presented in Table 2. Some important vibrational frequencies and the corresponding IR intensitives for the reactants, intermediates and transition states were listed in Table 3, and the frequencies were scaled by a factor of 0.963.[29] Experimental data indicated that the racemic α-amino nitriles would be produced in the absence of catalyst.[2,13] Therefore, the processes for the production of α-amino nitriles with (*S*) and (*R*) configuration might be similar. Thus, the following discussion was mainly focused on the pathways producing the (*S*)-enantiomer.

3.1. Investigations on the non-catalyzed Strecker reaction

As shown in Scheme 3, the calculations indicated that the racemic α-amino nitrile might be produced along two different reaction pathways (**a** and **b**), which was discussed, respectively, in detail as follows.

3.1.1. Pathway (a): isomerization followed by addition. The first reaction pathway (**a**) involved the isomerization of H_3SiCN to H_3SiNC firstly followed by the addition to $PhCH{=}NCH_3$ to produce the target α-amino nitrile via a five-membered ring transition state.

In this pathway, the calculations indicated that H_3SiCN was isomerized to H_3SiNC via a three-member ring transition state **TS1a** firstly. For **TS1a**, the distances of C and N to Si atom were 2.009 and 2.101 Å, respectively. The energy barrier for this step was as high as 30.4 kcal/mol, and the reactant H_3SiCN was 6.1 kcal/mol more stable than H_3SiNC. The possible isomerization process above in the present study was in agreement with the theoretical investigations on the mechanism of cyanide exchange for H_3SiCN reported by Wang et al.[30] The calculated characteristic vibrational frequencies for H_3SiCN and H_3SiNC were 2240 cm^{-1} (–C≡N stretch) and 2095 cm^{-1} (–N≡C stretch), respectively, which were close to the values of 2200 and 2098 cm^{-1} determined by Maier and

Table 1. Total energies E (Hartree), relative energies ΔE (kcal/mol) and relative Gibbs free energies ΔG (kcal/mol) in the gas phase and in CH_2Cl_2, respectively, for the stationary points

	E gas	ΔE gas	E solvent	ΔE solvent	ΔG solvent
Background reaction					
H_3SiCN	−384.10354		−384.13967		
$PhCH{=}NCH_3$	−364.85810		−365.01109		
H_3SiNC	−384.09432		−384.12988		
$H_3SiCN + PhCH{=}NCH_3$	−748.96164	0.0	−749.15076	0.0	0.0
TS1a + $PhCH{=}NCH_3$	−784.91636	28.4	−749.10228	30.4	29.1
$H_3SiNC + PhCH{=}NCH_3$	−748.95243	5.8	−749.14096	6.1	5.6
TS2a	−748.89653	40.9	−749.09574	34.5	48.3
P1a	−748.96962	−5.0	−749.162540	−7.4	7.8
TS1b	−748.89815	39.8	−749.096636	34.0	47.9
P1b	−748.94092	13.0	−749.133657	10.7	25.4
TS2b	−748.89799	39.9	−749.096039	34.3	47.2
Strecker reaction catalyzed by chiral *N*-oxide **B**					
B	−724.11569		−724.34517		
B + $H_3SiCN + PhCH{=}NCH_3$	−1473.07733	0.0	−1473.49593	0.0	0.0
$PhCH{=}NCH_3$ + **IM1c**	−1473.08636	−5.7	−1473.50682	−6.8	5.4
TS1c	−1473.04295	21.6	−1473.46747	17.9	47.3
IM2c	−1473.04750	18.7	−1473.47484	13.2	43.6
TS2c	−1473.03150	28.8	−1473.45976	22.7	52.9
IM3c	−1473.06116	10. 2	−1473.48223	8.6	35.8
B + **P1b**	−1473.05662	13.0	−1473.47882	10.7	25.4
TS2b + **B**	−1473.01369	39.9	−1473.44121	34.3	47.2
$PhCH{=}NCH_3$ + **TS1d**	−1473.04148	22.5	−1473.46064	22.1	33.1
$PhCH{=}NCH_3$ + **IM2d**	−1473.07641	0.6	−1473.49661	−0.4	10.3
TS2d	−1473.04004	23.4	−1473.46764	17.8	46.8
IM3d	−1473.04313	21.5	−1473.47161	15.3	45.8
TS3d	−1473.03115	29.0	−1473.46076	22.1	51.6
IM4d	−1473.08978	−7.8	−1473.51092	−9.4	18.0
B + **P1a**	−1473.08531	−5.0	−1473.50771	−7.4	7.8

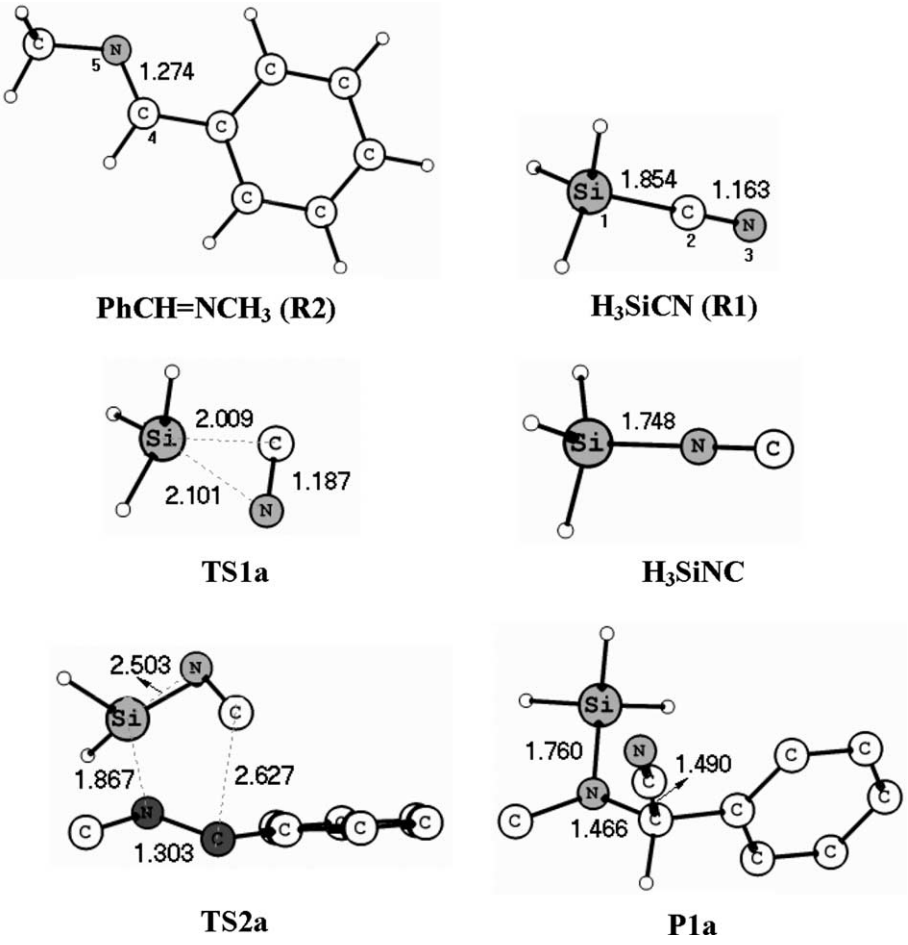

Figure 1. Optimized geometries of the stationary points along with pathway (**a**) in the absence of chiral *N*-oxide **B**.

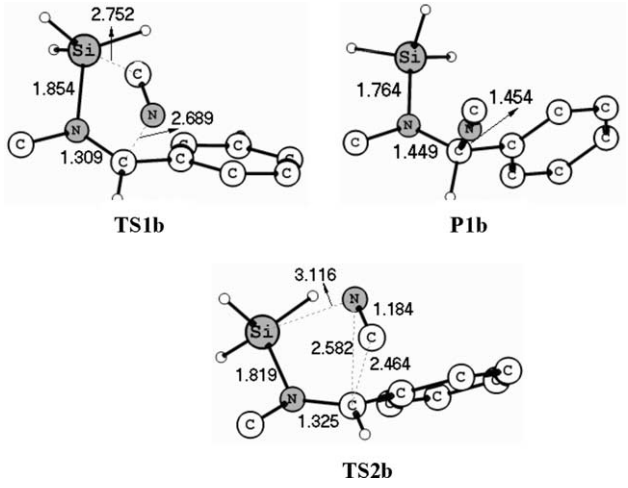

Figure 2. Optimized geometries of the stationary points along with pathway (**b**) in the absence of chiral *N*-oxide **B**.

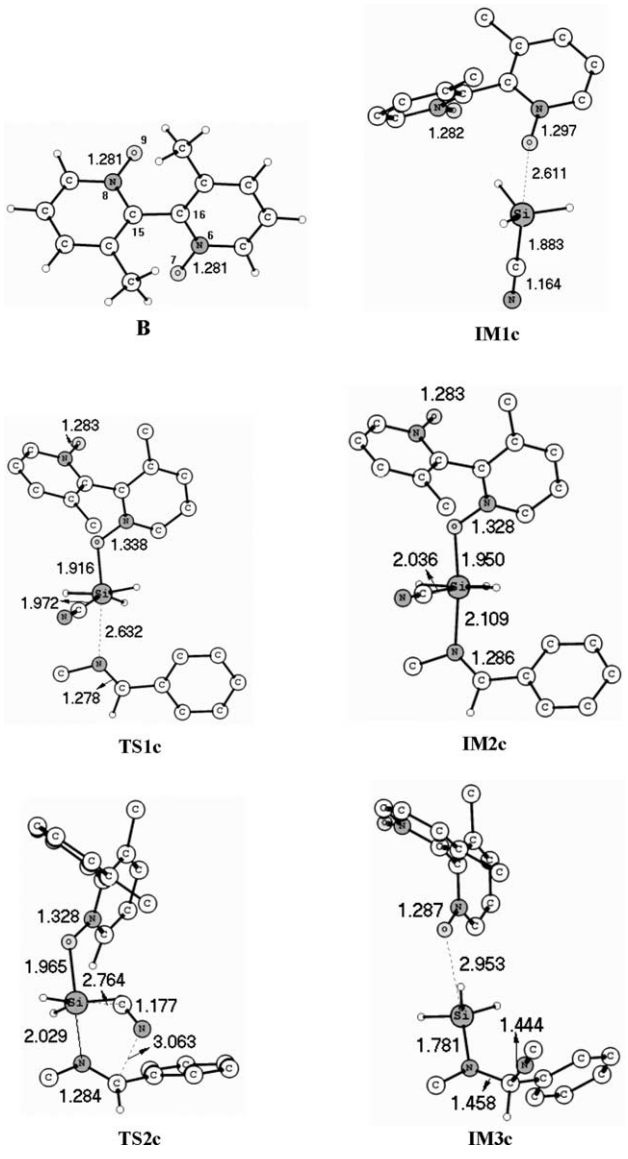

Figure 3. Optimized geometries of the stationary points along with pathway (**c**) in the presence of chiral *N*-oxide **B**.

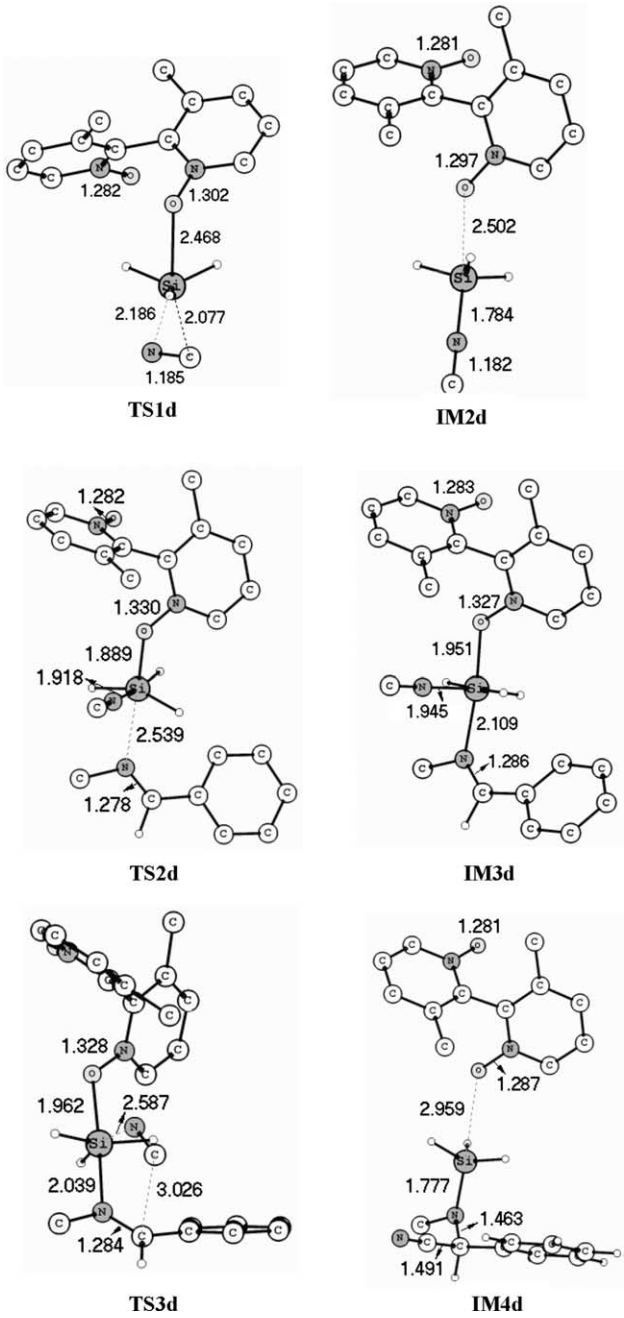

Figure 4. Optimized geometries of the stationary points along with pathway (**d**) in the presence of chiral *N*-oxide **B**.

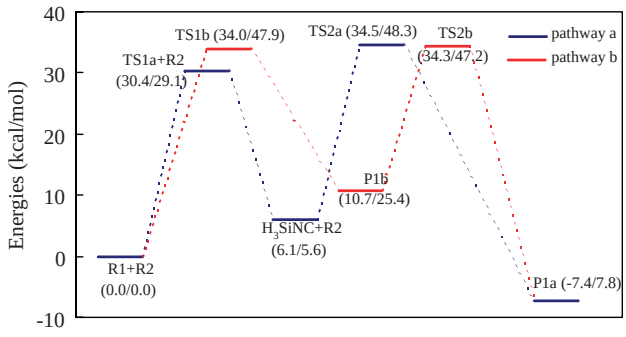

Figure 5. Relative energy/Gibbs free energy profiles for the Strecker reaction of PhCH=NCH$_3$ and H$_3$SiCN (in CH$_2$Cl$_2$) in the absence of chiral *N*-oxide **B** along the pathway (**a**) and (**b**) at the B3LYP/6-31G* level.

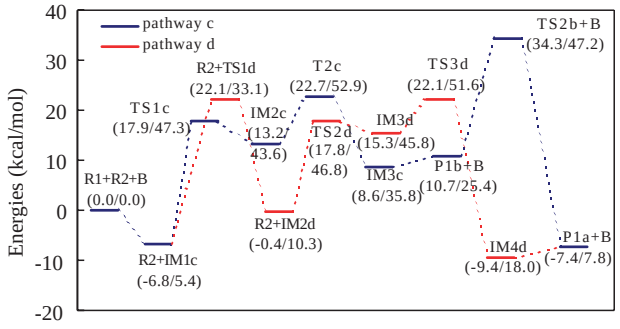

Figure 6. Relative energy/Gibbs free energy profiles for the Strecker reaction of PhCH═NCH_3 and H_3SiCN (in CH_2Cl_2) catalyzed by chiral *N*-oxide **B** along pathway (**c**) and (**d**) at the B3LYP/6-31G* level.

co-workers from photochemical experiments.[31] These results indicated that the present theoretical method of B3LYP/6-31G* was appropriate for this system. In order to testify the efficiency of the modeling molecule, the isomerization process for real reactant $(CH_3)_3SiCN$ was also investigated. Calculations indicated that the process of isomerization from TMSCN to TMSNC was similar to that for modeling molecule H_3SiCN. The energy barrier for the isomerization of TMSCN was 30.0 kcal/mol in CH_2Cl_2 and 27.9 kcal/mol in gas phase, respectively, which were close to those for H_3SiCN (30.4 kcal/mol in CH_2Cl_2 and 28.4 kcal/mol in gas phase).

In the following step, the α-amino nitrile would be obtained by the addition of H_3SiNC to PhCH═NCH_3 via the transition state **TS2a**. The calculation gave an exothermicity of about

Table 2. Selected Wiberg bond indices for the stationary points at the B3LYP/6-31G* level

	N8–O9	N6–O7	Si1–C2	C2–N3	C4–N5	Si1–O7	Si1–N3	Si1–N5	C2–C4	N3–C4
B	1.281	1.281								
R1					1.844					
R2			0.846							
TS1a			0.538				0.333			
H_3SiNC							0.656			
TS2a					1.576			0.512	0.117	
P1a					0.973			0.679	1.011	
TS1b			0.201		1.539			0.521		0.069
P1b					1.003			0.675		0.915
TS2b					1.442			0.568	0.176	0.125
IM1c	1.278	1.217	0.797	2.938		0.078				
TS1c	1.276	1.091	0.635	2.902	1.815	0.368		0.147		
IM2c	1.276	1.118	0.562	2.899	1.753	0.335		0.317		
TS2c	1.271	1.117	0.196	2.855	1.736	0.325		0.356		0.010
IM3c	1.280	1.256		2.411	1.014	0.048		0.627		0.908
TS1d	1.280	1.197	0.480				0.279			
IM2d	1.282	1.217		2.421		0.111	0.592			
TS2d	1.278	1.100		2.541	1.809	0.368	0.414	0.167		
IM3d	1.277	1.121		2.570	1.755	0.336	0.397	0.315	0.003	
TS3d	1.270	1.118		2.700	1.734	0.326	0.147	0.351	0.024	
IM4d	1.280	1.257		2.912	0.981	0.047		0.633	1.011	

Table 3. Selected vibrational frequencies (cm^{-1}) and IR intensities (Debye^2/amu Å^2) for all the species involved in the reaction of H_3SiCN and PhCH═NCH_3 catalyzed by chiral *N*-oxide **B**

	Frequencies (cm^{-1})/IR intensities, Debye^2/amu (Å^2)									
	N8–O9	N6–O7	Si1–C2	C≡N	C4–N5	Si1–O7	Si1–N3	Si1–N5	C2–C4	N3–C4
B	1309/179.5	1309/179.5								
R1			581/36.6	2240/10.3						
R2					1679/85.0					
TS1a			517/96.7	2015/5.4						
H_3SiNC				2095/294.3			650/66.6			
TS2a				2065/45.7	1594/222.3			559/4.8		
P1a				2262/1.5	1189/35.1			649/12	912/22.2	
TS1b				2070/22.8	1561/221.8			571/7.9		
P1b				2123/130.5	1196/67.9			648/12.1		895/93.3
TS2b				2037/14.2	1525/273.3			629/6.8		
IM1c	1281/132.7	1311/85.3	538/140.7	2228/5.8		49/2.1				
TS1c	1217/25.9	1312/80.0	429/93.2	2182/2.7	1666/122	591/71.3				
IM2c	1224/44.6	1312/78.8	412/41.3	2173/0.3	1650/165.8	593/86.6		271/58		
TS2c	1227/36.3	1309/76.3		2095/6.8	1655/183.5	591/75.9		280/128.9		
IM3c	1300/172.8	1314/60.9		2121/129.6	1198/84.8			643/10		881/95.5
TS1d	1274/120.7	1311/84.6	428/291.5	2030/5.2						
IM2d	1283/139.8	1314/83.5		2097/335.6		44/14.0				
TS2d	1234/47.4	1310/8/0.2		2092/154.4	1665/113.9	613/131.9	398/77.2			
IM3d	1225/37.9	1313/78.2		2101/118.1	1651/159.9	593/91.2	414/66.1	289/51.0		
TS3d	1227/35.8	1308/76.4		2055/37.1	1654/167.3	591/82.2		279/44.9		
IM4d	1301/173.6	1314/60.2		2258/2.3	1198/84.8			646/8.9	908/55.6	

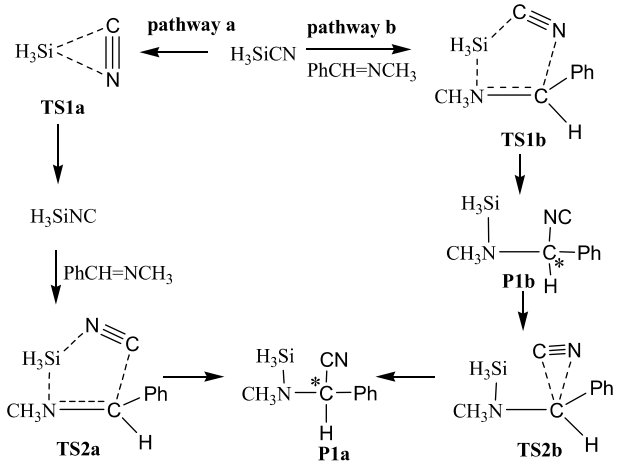

Scheme 3. Two different reaction pathways (**a** and **b**) to produce α-amino nitrile in the absence of a catalyst.

13.5 kcal/mol, and an energy barrier of 28.4 kcal/mol for this step. For **TS2a**, the Si1–N5 distance of 1.867 Å was close to that for the product **P1a** (1.760 Å). The distance of N5–C4 was remarkably larger than that of the reactant, and the Wiberg bond index of N5–C4 bond was decreased from 1.844 to 1.576. These results indicated that the N=C double bond for the imine was intensively weakened in the transition state **TS2a**. The transition vector of the unique imaginary frequency indicated that the C2 of –CN group got gradually close to C4 and N3 of –CN group moved away from Si1, indicating that the transition state obtained was actually connected with the starting reactant and terminating product as expected.

3.1.2. Pathway (b): addition followed by isomerization. The second reaction pathway to provide the target product α-amino nitrile involved two steps. Firstly, H_3SiCN was reacted with $PhCH{=}NCH_3$ to produce α-amino isonitrile via the transition state **TS1b**. Subsequently, α-amino isonitrile (**P1b**) would be isomerized to α-amino nitrile (**P1a**) via the transition state **TS2b**.

For the transition state **TS1b**, the N5–C4 distance was increased from 1.274 to 1.309 Å, indicating that C=N double bond had been weakened. The Si1–C2 and N3–C4 distances were 2.752 and 2.689 Å, respectively. The energy barrier for the addition of H_3SiCN to $PhCH{=}NCH_3$ was 5.6 kcal/mol higher than that for the addition of H_3SiNC to $PhCH{=}NCH_3$. It was turned out that H_3SiNC was more reactive than H_3SiCN though the former was less stable than the latter.

Next, α-amino isonitrile (**P1b**) would be isomerized to α-amino nitrile (**P1a**) via the transition state **TS2b**. **TS2b** beared close resemblance to **TS2a**, but the distance of N3–Si1 in **TS2b** was 3.116 Å, longer than that in **TS2a**. Si1 atom in **TS2b** was closer to N5 atom than that in **TS2a**, and the vibrational mode of the unique imaginary frequency of 201 cm^{-1} indicated that N3 moved away from C4 and C2 got close to C4 atom.

3.1.3. The mechanism of the non-catalyzed reaction. *Comparison of the activity between H_3SiCN and H_3SiNC*

The facile equilibrium between C-bonded and N-bonded cyanotrialkylsilane has been verified by the spectroscopic studies of Booth and Frankiss.[32] Although the equilibrium concentration of isocyanide in the organic solution is generally low, it is possible for H_3SiNC to participate in the reaction of cyanosilylation of aldimines as a silylcyanide reagent. The positive charge accumulated on Si atom in H_3SiNC is larger than that in H_3SiCN, indicating stronger electrophilicity of Si atom in H_3SiNC. As a result, H_3SiNC may carry out addition reaction more easily than H_3SiCN, which can be verified by the lower energy barrier for the addition of –NC group to C=N double bond. Therefore, H_3SiNC is more reactive than H_3SiCN in the reaction of cyanosilylation of aldimines, and a greater electropositive character of the silicon atom in H_3SiNC has been suggested to be responsible for its increased reactivity.

Comparison of the two pathways for the non-catalyzed Strecker reaction

It was noted that the structure of **TS1b** obtained in the present calculation was similar to that of the transition state obtained by Cativiela et al.[22] However, the intermediate containing high coordinated silicon atom presumed by Cainelli et al.[33] was not located as a minimum in the present work. According to the NBO analysis, there were strong interactions between Si1–C2–N3–C4–N5 (or Si1–N3–C2–C4–N5) five atoms in the transition states **TS1b** (or **TS2a**). Therefore, it was reasonable to consider that the reaction was a concerted one, forming five-membered ring transition state. The calculations predicated that the energy barriers of RDS for pathway (**a**) and (**b**) were 35.1 and 39.8 kcal/mol, respectively, and the rate-determining-step (RDS) for both pathways (**a**) and (**b**) was the nucleophilic attack step, that is, the addition of –NC or –CN groups to C=N double bond in the gas phase. Compared with the results obtained in gas phase, the solvent effects significantly lowered the energy barrier of the RDS in CH_2Cl_2 (the energy barrier of the RDS for pathway (**a**) was 30.4 kcal/mol, while that for pathway (**b**) was 34.0 kcal/mol). As shown in Figure 5, the calculations predicted that the relative energies of the highest transition states for pathway (**a**) and (**b**) were similar either in the solvent or in the gas phase. Thus two reaction pathways were competitive with comparable energy maximum. In general, the energy barriers for the addition of –CN or –NC group to C=N double bond were very high for both pathway (**a**) and (**b**) in the absence of a catalyst.

3.2. Investigations on the Strecker reaction catalyzed by chiral *N*-oxide B

It was found experimentally that chiral *N*-oxides were catalytically active for asymmetric cyanosilylation of aldimines.[2,13] The calculations indicated that the production of α-amino nitrile would be realized along two different reaction pathways (**c** and **d**) (as shown in Scheme 4) catalyzed by chiral *N*-oxide **B**, in which the chiral *N*-oxide **B** played a key role to lower the energy barriers of the addition for –CN or –NC group to C=N double bond.

3.2.1. Pathway (c): addition followed by isomerization. In this pathway, H_3SiCN was coordinated to the chiral *N*-oxide **B** and then reacted with $PhCH{=}NCH_3$ to form hexacoordinate silicon species. Next, the cyano group attacked the imine to produce the α-amino isonitrile, which was then isomerized to target α-amino nitrile.

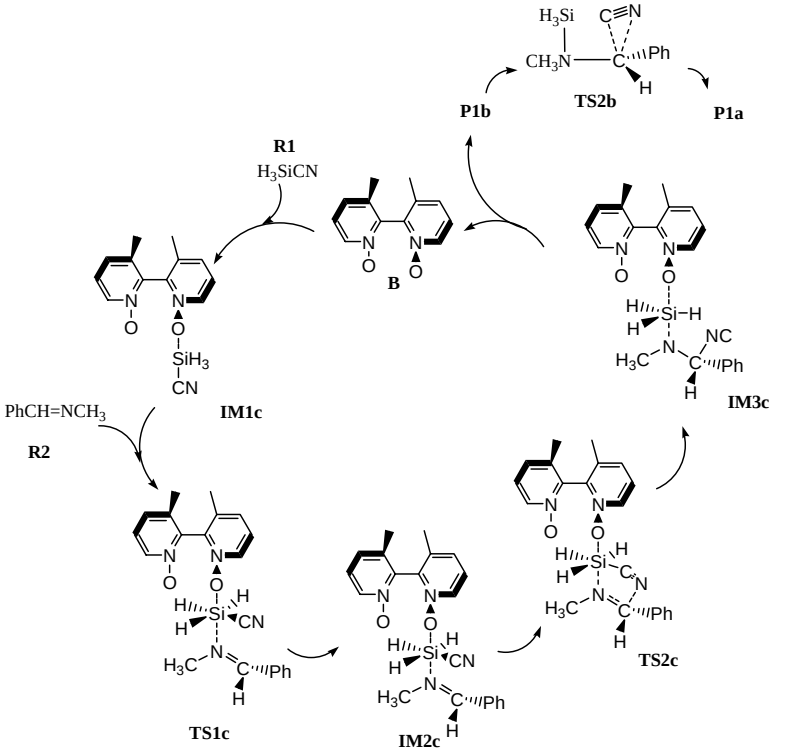

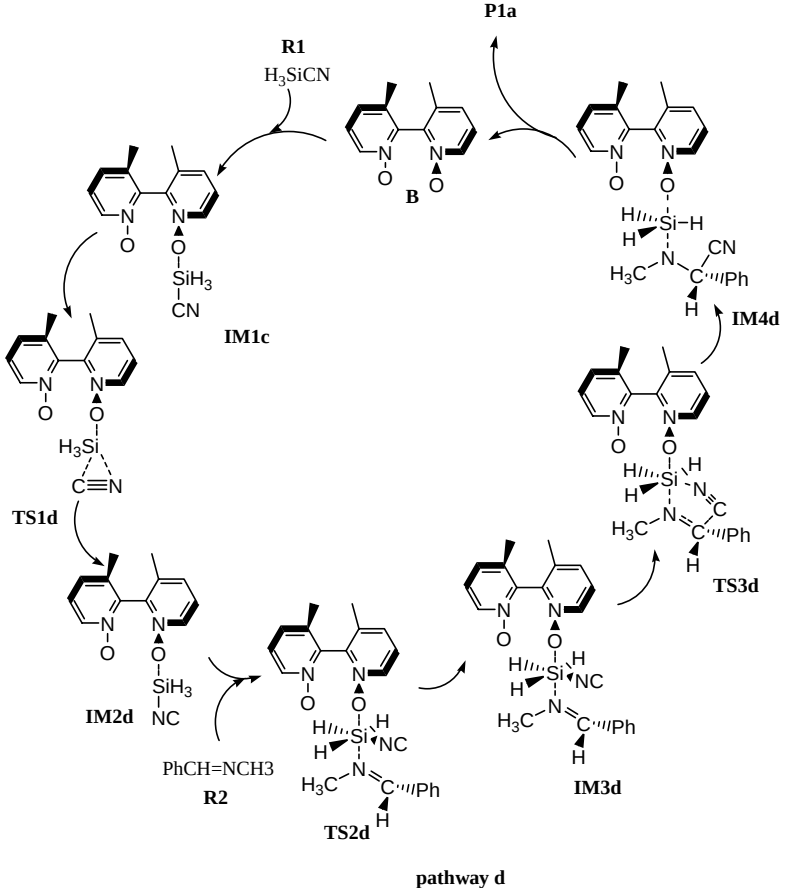

Scheme 4. Two different reaction pathways (**c** and **d**) to produce α-amino nitrile (**P1a**) in the presence of chiral *N*-oxide **B**.

For the reaction pathway (**c**), chiral *N*-oxide **B** was interacted firstly with H_3SiCN, leading to the formation of binary molecular complex **IM1c**, which was stabilized by the interaction between O atom of chiral *N*-oxide **B** and the Si atom of H_3SiCN. For the **IM1c**, the N6–O7 bond interacting directly with H_3SiCN became longer (1.281→1.297 Å), and the negative charge on O7 was increased (−0.529*e*→−0.570*e*). The Si1–C2 distance was longer than that of free H_3SiCN, indicating that Si1–C2 chemical bond was weakened in the binary molecular complex. The charge for the H_3SiCN moiety was −0.06*e*, indicating that the formation of **IM1c** resulted in partial charge transfer from the chiral *N*-oxide **B** moiety to the H_3SiCN moiety. It should be noted that the binary molecular complex **IM1c** was somewhat different from the hypothetical one proposed experimentally, in which the formation of six-coordination hypervalent silicate species by coordinating two O atoms of chiral *N*-oxide to Si atom of TMSCN simultaneously was proposed.[13]

Then, PhCH=NCH_3 was drawn close to the **IM1c** to form stable intermediate **IM2c** via the transition state **TS1c**. This step involved an energy barrier of 24.7 kcal/mol. For the intermediate **IM2c**, C4–N5 and Si1–C2 distances were elongated remarkably, and the Wiberg bond indices of Si1–C2 and C4–N5 were decreased. These results indicated that Si1–C2 and C4–N5 bonds were activated remarkably. **IM2c** was a hexacoordinate silicon species with a greater electropositive character on the hypervalent silicon atom, indicating the increased polarity for Si1–C2 bond. The increase of negative charge on –CN group indicated that the nucleophilicity of –CN group was enhanced.

Next, the highly reactive cyano group attacked the imine to produce **IM3c** via the transition state **TS2c**. The energy barrier for this step was 9.5 kcal/mol, which was remarkably lower than that for the background reaction. For the transition state **TS2c**, Si1–C2 and N3–C4 distances were 2.764 and 3.063 Å, respectively. The vibrational mode of the unique imaginary frequency of 125 cm^{-1} was corresponding to that cyano group was gradually closer to C4 and further away from Si1.

Intermediate **IM3c** could be regarded as the complex formed by chiral *N*-oxide **B** and α-amino isonitrile. The geometrical structure of α-amino isonitrile moiety was very similar to that of free α-amino isonitrile (**P1b**). In the following step, the chiral *N*-oxide **B** was regenerated by leaving the α-amino isonitrile moiety with 2.1 kcal/mol energy gain respected to **IM3c**. The α-amino isonitrile (**P1b**) would be isomerized to target product α-amino nitrile (**P1a**), which was the same as the isomerization process in the pathway (**b**) without chiral *N*-oxide **B**.

3.2.2. Pathway (d): isomerization followed by addition. The calculations indicated that the target product—α-amino nitrile (**P1a**) could also be obtained along with the competitive reaction pathway (**d**), in which H_3SiCN was isomerized to H_3SiNC initially catalyzed by chiral *N*-oxide **B** to produce the intermediate **IM2d**. The energy barrier for the catalytic isomerization of H_3SiCN to H_3SiNC was slightly lower than that without the catalyst, and the energy difference between the binary complexes of H_3SiCN and H_3SiNC with the chiral *N*-oxide **B** was 6.4 kcal/mol, which was slightly higher than the energy difference of 6.1 kcal/mol between H_3SiCN and H_3SiNC. Therefore, the chiral *N*-oxide **B** exerted little influence on the isomerization of H_3SiCN to H_3SiNC.

For the transition state **TS1d**, Si1–C2 and Si1–N3 distances were 2.077 and 2.186 Å, respectively, longer than those for **TS1a**. NBO analysis indicated that there existed interaction in the Si1–C2–N3 three-member ring. Though the energy barrier for this step was rather high, the intermediate **IM2d** was more reactive than **IM1c** because of the greater electropositive character of Si atom. The possibility for the formation of isocyanide as a reactive intermediate in the reaction has also been reported recently in some experimental investigations.[34,35]

For **IM2d**, the higher Wiberg bond index than that for **IM1c** indicated that there was strong interaction between O7–Si1. This effect would weaken the interaction between Si1–N3 and lead to the elongation of Si1–N3 bond. In the following step, PhCH=NCH_3 was drawn close to **IM2d** to form the intermediate **IM3d** via the transition state **TS2d**. The energy barrier for this step was 18.2 kcal/mol.

IM3d was a hexacoordination silicate similar to that for **IM2c**. However, the natural charge for –NC group was −0.693*e*, which was greater than the corresponding value for **IM2c**. This result indicated that the nucleophilicity for –NC group in **IM3d** was stronger than that for –CN group in **IM2c**, which could be verified by the lower energy barrier to carry out nucleophilic attack for imine via the transition state **TS3d**.

The structure of **IM4d** could be regarded as the molecular complex formed by chiral *N*-oxide **B** and the target product α-amino nitrile. In the final step, the chiral *N*-oxide **B** was cleaved from the α-amino nitrile moiety by 2.0 kcal/mol energies gain with respect to **IM4d**.

3.2.3. The reaction mechanism catalyzed by chiral *N*-oxides B. *Comparison of two reaction pathways*. Two competitive pathways (**c** and **d**) for the reaction of H_3SiCN and PhCH=NCH_3 catalyzed by chiral *N*-oxide **B** to furnish α-amino nitrile were rationalized. In the reaction pathway (**c**), the step corresponding to the formation of the three-member complex **IM2c** was predicted to be the rate-determining-step (RDS). In the pathway (**d**), the reaction step from **IM1c** to **IM2d**, which was corresponded to the step of the H_3SiCN isomerizing to H_3SiNC catalyzed by chiral *N*-oxide **B**, was predicted to be the rate-determining-step (RDS) in CH_2Cl_2. Compared with the results obtained in gas phase, the energy barriers of RDS of 24.7 kcal/mol for pathway (**c**) in solvent was lower than the corresponding RDS of pathway (**d**). Although the energy barrier of RDS for pathway (**d**) calculated in CH_2Cl_2 was slightly higher than that in gas phase, the energy maximum along the reaction pathway (**d**) (22.1 kcal/mol for **TS1d**+**R2**) was lower than the energy maximum along the reaction pathway (**c**) (34.3 kcal/mol for **TS2b**). Thus, the solvent had exerted significant influences on the reaction.

Role of the chiral N-oxides **B**. In contrast to carbon, silicon has a marked tendency to increase its coordination number,

and the structures for some penta- and hexacoordinate silicon compounds have been characterized by X-ray diffraction.[36,37] Though the classification of chemical bonds in the multicoordinate silicon remains controversial,[38] the enhanced reactivity for them have been proved by experimental data.[36,37,39] Since amine *N*-oxides are known to exhibit a significant nucleophilicity toward the silicon, some hypervalent silicate intermediates or transition states formed by the O atom of amine *N*-oxides coordinating to Si atom have been proposed in some processes using amine *N*-oxides as the catalyst.[13,15,40,41] For the Strecker reaction between aldimines and trimethylsilyl cyanide catalyzed by chiral *N*-oxides, a mechanistic hypothesis involving the hexacoordinate hypervalent silicate intermediate has been suggested.[13]

The present calculations predicted that chiral *N*-oxide **B** had C_2 symmetry and its dihedral angle of $D_{8\text{–}15\text{–}16\text{–}6}$ was $-113.2°$. The N–O bond was coplanar with aromatic rings in the quinoline and there existed conjugative interactions between them. However, N^+–O^- group was strongly polarizable and the electron density on O atom was higher, which facilitated O atom to interact with the Si atom. This effect would weaken the Si1–C2 bond, leading to the elongation of Si1–C2 distance. As a result, the energy barrier of the isomerization from cyano to isocyano for H_3SiCN moiety was lowered. Compared with the charge on the Si atom for binary complexes of **IM1c** and **IM2d**, the larger electropositive character for Si1 in **IM2d** indicated its stronger electrophilicity, which was in agreement with the lower energy barrier for **IM2d** to form hexacoordinate silicate **IM3d**.

Three-membered complexes **IM3d** and **IM2c** shown in Figures 3 and 4 displayed a similar and somewhat distorted octahedral geometry. Six atoms in the H_3SiCN were almost in the same plane, and the chiral *N*-oxide **B** and imine with larger volume occupied the axial position. Si1–O7 and Si1–N5 distances were in the range normally observed for hexacoordinate silicon compounds.[36] Therefore, they could be treated as hexacoordinate silicate species. Based on the larger Wiberg bond indices for Si1–O7 and Si1–N5, there was strong interactions between chiral *N*-oxide **B** and imine with H_3SiCN, which led to the changes of the stretching modes for N6–O7 of chiral *N*-oxide **B** participating in coordination and for C=N double bond of imine. According to the vibrational analysis, frequencies of 1313 and 1312 cm^{-1}, which were assigned to the asymmetric stretching modes of N6–O7 for **IM3d** and **IM2c**, respectively, were lower than that for free chiral *N*-oxide **B**. Frequencies of 1651 and 1650 cm^{-1}, which were assigned to the asymmetric stretching modes of C=N bond for **IM3d** and **IM2c**, respectively, were lower than that for free imine. According to atomic natural charges of **IM3d** and **IM2c**, there was a charge transfer from O atom of chiral *N*-oxide **B** and N atom of imine to H_3SiCN moiety, and afterward it resulted in a total transfer of 0.342*e* for **IM3d** and 0.357*e* for **IM2c**, respectively, from *N*-oxide **B** and imine moieties to H_3SiCN moiety. This effect would strengthen the interactions between O7 and N5 atoms with Si1 atom and weaken the interaction between Si1 and –NC or –CN group, leading to the elongation of the Si–N(C) or Si–C(N) bond. Simultaneously, the nucleophilicities of the isocyano group or cyano group were enhanced. Consequently, the energy barriers for the attack of –NC or –CN group to C4 atom of imine were lower remarkably than that in the absence of chiral *N*-oxide **B**.

In all, chiral *N*-oxide played a key role for the initial activation of Si–C bond by coordinating O atom to Si atom of silyl cyanide (or silyl isocyanide) and the stabilization of three-membered complex (**IM2c** and **IM3d**). As a result, the energy barrier was decreased remarkably and the reaction was carried out more easily. The formation of hexacoordinate silicate species was very important for the activation of Si1–C2 or Si1–N3 bond, making –CN (or –NC) group more nucleophilic.

4. Conclusion

The main results can be summarized as follows:

1. For the background reaction in the absence of chiral *N*-oxide **B** catalyst, the racemic α-amino nitrile may be produced along two different reaction pathways. The calculations indicated that the two reaction pathways were competitive with comparable energy maximum.
2. For the reaction catalyzed by chiral *N*-oxide **B**—3,3′-dimethyl-2,2′-bipyridine *N*,*N*′-dioxide, although the energy barriers of RDS for pathway (**c**) in solvent was lower than the corresponding RDS of pathway (**d**), the energy maximum along the reaction pathway (**d**) (22.1 kcal/mol for **TS1d**+**R2**) was lower than the energy maximum along the reaction pathway (**c**) (34.3 kcal/mol for **TS2b**). Thus, the two reaction pathways were also comparable.
3. The strong electron donor (N–O) of chiral *N*-oxide **B** played an important role in enhancing reactivity and nucleophilicity of H_3SiCN. The hexacoordinate hypervalent silicate was a stable intermediate. The formation of such hexacoordinate hypervalent silicate intermediate could enhance intensively the nucleophilicity of –NC or –CN group and lower the energy barriers of addition reaction. As a consequence, it facilitated the production of the target α-amino nitrile.

In short, the information obtained from the present work may be useful to investigate further the origin of chiral control for chiral *N*-oxide and provide some hints for the design and synthesis of novel chiral *N*-oxides catalysts for Strecker reaction.

Acknowledgements

We thank the National Science Foundation of China (Nos. 20225206, 20390055, and 20372050), the Ministry of Education of China (No. 104209 and others), the Teaching and Research Award Program for Outstanding Young Teachers in Higher Education Institutions of M.O.E. (2002), P.R.C., and Sichuan University (No. 2004CF07) for financial support.

References and notes

1. Ishitani, H.; Komiyama, S.; Hasegawa, Y.; Kobayashi, S. *J. Am. Chem. Soc.* **2000**, *122*, 762–766.
2. Liu, B.; Feng, X.; Chen, F.; Zhang, G.; Cui, X.; Jiang, Y. *Synlett* **2001**, *10*, 1551–1554.
3. Strecker, A. *Ann. Chem. Pharm.* **1850**, *75*, 27–45.
4. Shafran, Y. M.; Bakulev, V. A.; Mokrushin, V. S. *Russ. Chem. Rev.* **1989**, *58*, 148–162.
5. Iyer, M. S.; Gigstad, K. M.; Namdev, N. D.; Lipton, M. *J. Am. Chem. Soc.* **1996**, *118*, 4910–4911.
6. Corey, E. J.; Grogan, M. J. *Org. Lett.* **1999**, *1*, 157–160.
7. Vachal, P.; Jacobsen, E. N. *Org. Lett.* **2000**, *2*, 867–870.
8. Yet, L. *Angew. chem*. **2001**, *113*, 900–902; *Angew. Chem., Int. Ed*. **2001**, **40**, 875–877.
9. Sigman, M. S.; Jacobsen, E. N. *J. Am. Chem. Soc.* **1998**, *120*, 5315–5316.
10. Takamura, M.; Hamashima, Y.; Usuda, H.; Kanai, M.; Shibasaki, M. *Angew. Chem*. **2000**, *112*, 1716–1718; *Angew. Chem. Int. Ed*. **2000**, *39*, 1650–1652.
11. Sigman, M.S.; Vachal, P.; Jacobsen, E. N. *Angew. Chem*. **2000**, *112*, 1336–1338; *Angew. Chem. Int. Ed*. **2000**, *39*, 1279–1281.
12. Josephsohn, N. S.; Kuntz, K. W.; Snapper, M. L.; Hoveyda, A. H. *J. Am. Chem. Soc.* **2001**, *123*, 11594–11599.
13. Jiao, Z.; Feng, X.; Liu, B.; Chen, F.; Zhang, G. L.; Jiang, Y. *Eur. J. Org. Chem.* **2003**, 3818–3826.
14. Karayannis, N. M.; Pytlewski, L. L.; Mikulski, C. M. *Coord. Chem. Rev.* **1973**, *11*, 93–159.
15. Chelucci, G.; Murineddu, G.; Pinna, G. A. *Tetrahedron: Asymmetry* **2004**, *15*, 1373–1389.
16. Eller, K.; Schwarz, H. *Chem. Rev.* **1991**, *91*, 1121–1177.
17. Armentrout, P. B. *Science* **1991**, *251*, 175–179.
18. Roth, L. M.; Freiser, B. S. *Mass Spectrom. Rev.* **1991**, *10*, 303–328.
19. Weisshaar, J. C. *Acc. Chem. Res.* **1993**, *26*, 213–219.
20. Yoshihiti, S.; Kazunari, Y. *J. Am. Chem. Soc.* **2000**, *122*, 12317–12326.
21. Hwang, D. Y.; Mebel, A. M. *J. Phys. Chem. A* **2003**, *107*, 5092–5100.
22. Cativiela, C.; Díaz-de-Villegas, M. D.; Gálvez, J. A.; García, J. I. *Tetrahedron* **1996**, *52*, 9563–9574.
23. Li, J.; Jiang, W.; Han, K.; He, G.; Li, C. *J. Org. Chem.* **2003**, *68*, 8786–8789.
24. Vachal, P.; Jacobsen, E. N. *J. Am. Chem. Soc.* **2002**, *124*, 10012–10014.
25. Arnaud, R.; Adamo, C.; Cossi, M.; Milet, A.; Vallée, Y.; Barone, V. *J. Am. Chem. Soc.* **2000**, *122*, 324–330.
26. Frisch, M. J.; Trucks, G. W.; Schlegel, H. B.; Scuseria, G. E.; Robb, M. A.; Cheeseman, J. R.; Montgomery, J. A., Jr.; Vreven, T.; Kudin, K. N.; Burant, J. C.; Millam, J. M.; Iyengar, S. S.; Tomasi, J.; Barone, V.; Mennucci, B.; Cossi, M.; Scalmani, G.; Rega, N.; Petersson, G. A.; Nakatsuji, H.; Hada, M.; Ehara, M.; Toyota, K.; Fukuda, R.; Hasegawa, J.; Ishida, M.; Nakajima, T.; Honda, Y.; Kitao, O.; Nakai, H.; Klene, M.; Li, X.; Knox, J. E.; Hratchian, H. P.; Cross, J. B.; Adamo, C.; Jaramillo, J.; Gomperts, R.; Stratmann, R. E.; Yazyev, O.; Austin, A. J.; Cammi, R.; Pomelli, C.; Ochterski, J. W.; Ayala, P. Y.; Morokuma, K.; Voth, G. A.; Salvador, P.; Dannenberg, J. J.; Zakrzewski, V. G.; Dapprich, S.; Daniels, A. D.; Strain, M. C.; Farkas, O.; Malick, D. K.; Rabuck, A. D.; Raghavachari, K.; Foresman, J. B.; Ortiz, J. V.; Cui, Q.; Baboul, A. G.; Clifford, S.; Cioslowski, J.; Stefanov, B. B.; Liu, G.; Liashenko, A.; Piskorz, P.; Komaromi, I.; Martin, R. L.; Fox, D. J.; Keith, T.; Al-Laham, M. A.; Peng, C. Y.; Nanayakkara, A.; Challacombe, M.; Gill, P. M. W.; Johnson, B.; Chen, W.; Wong, M. W.; Gonzalez, C.; Pople, J. A. *Gaussian 03*, Revision B.05; Gaussian, Inc.: Pittsburgh, PA, 2003.
27. Cossi, M.; Barone, V.; Mennucci, B.; Tomasi, J. *Chem. Phys. Lett.* **1998**, *286*, 253–260.
28. (a) Reed, A. E.; Curtiss, L. A.; Weinhold, F. *Chem. Rev.* **1988**, *88*, 899–926. (b) Reed, A. E.; Weinstock, R. B.; Weinhold, F. *J. Chem. Phys.* **1985**, *83*, 735–746.
29. Pople, J. A.; Scott, A. P.; Wong, M. W.; Radom, L. *Isr. J. Chem.* **1993**, *33*, 345–350.
30. Wang, Q.; Ding, Y.; Sun, C. *J. Phys. Chem. A* **2004**, *108*, 10602–10608.
31. Maier, G.; Reisenauer, H. P.; Egenolf, H.; Glatthaar, J. *Eur. J. Org. Chem.* **1998**, 1307–1311.
32. Seckar, J. A.; Thayer, J. S. *Inorg. Chem.* **1976**, *15*, 501–504.
33. Cainelli, G.; Giacomini, D.; Treré, A.; Galletti, P. *Tetrahedron: Asymmetry* **1995**, *6*, 1593–1600.
34. Ryu, D. H.; Corey, E. J. *J. Am. Chem. Soc.* **2004**, *126*, 8106–8107.
35. Cheng, F.; Zhou, H.; Liu, X.; Qin, B.; Feng, X.; Zhang, G.; Jiang, Y. *Chem. Eur. J.* **2004**, *10*, 4790–4797.
36. Chuit, C.; Corrlu, R. J. P.; Reye, C.; Young, J. C. *Chem. Rev.* **1993**, *93*, 1371–1448.
37. Nakash, M.; Goldvaser, M. *J. Am. Chem. Soc.* **2004**, *126*, 3436–3437.
38. Kocher, N.; Henn, J.; Gostevskii, B.; Kost, D.; Kalikhman, I.; Engels, B.; Stalke, D. *J. Am. Chem. Soc.* **2004**, *126*, 5563–5568.
39. Deiters, J. A.; Holmes, R. R. *J. Am. Chem. Soc.* **1990**, *112*, 7197–7202.
40. Sato, K.; Kira, M.; Sakurai, H. *Tetrahedron Lett.* **1989**, *30*, 4375–4378.
41. Nakajima, M.; Saito, M.; Shiro, M.; Hashimoto, S. *J. Am. Chem. Soc.* **1998**, *120*, 6419–6420.